Textile-Integrated ZnO-Based Thermoelectric Device Using Atomic Layer Deposition

Giovanni Marin, Ryoji Funahashi, and Maarit Karppinen*

Herein, a full thermoelectric (TE) device fabricated on textile using atomic layer deposition (ALD) and molecular layer deposition (MLD) thin-film techniques is demonstrated. The device consists of n-type ALD-grown ZnO or ALD/MLD-grown ZnO-organic components and p-type spray/immersion-coated PEDOT:PSS components. Different fabrication strategies and device designs (vertical and longitudinal) are investigated. The performance is evaluated by measuring the open-circuit voltage generated by the device over a range of temperature differences (between the hot and cold sides) up to 60 °C. At a fixed ΔT, the voltage generated is found to increase with increasing ZnO or ZnO-organic film thickness. An attractive feature with both ALD and MLD is that the film grows in a conformal manner on the textile fibers so that the entire textile piece becomes an active part of the device, corresponding to a remarkable coating-thickness increase. The voltage generated can also be increased by combining more TE pairs (even by just increasing the number of pairs by cutting the TE pads into smaller pieces). This research has thus proven the feasibility of ALD and MLD techniques in combination with a textile substrate in reinforcing the prospects of wearable thermoelectrics.

1. Introduction

The continuously increasing interest in lightweight and flexible low-power solutions for self-powered mobile electronics and sensors required in the rapidly expanding application sectors such as wearable electronics and implantable health monitoring systems[1–5] has in recent years propelled the research on various local energy harvesting technologies.[6–10] As the potential ubiquitous energy harvesting methods to provide supplemental

G. Marin, Prof. M. Karppinen
Department of Chemistry and Materials Science
Aalto University
FI-00076 Aalto, Finland
E-mail: maarit.karppinen@aalto.fi

Prof. R. Funahashi
Nanomaterials Research Institute
National Institute of Advanced Industrial Science and Technology (AIST)
Osaka 563-8577, Japan

The ORCID identification number(s) for the author(s) of this article can be found under https://doi.org/10.1002/adem.202000535.

or backup power, three technologies in particular have been investigated, i.e., thermoelectricity, piezoelectricity, and triboelectricity. Among these technologies, thermoelectricity is an ideal choice for personalized devices, as it can be harnessed to directly convert body heat into electric power.[11–13] Thin-film thermoelectric devices in particular could be integrated with energy storage devices (batteries) to enhance the service life of wearable devices.[14]

The variety of new flexible thermoelectric (TE) materials is rapidly increasing to cover, for example, a range of different conductive polymers[15,16] and multilayered inorganic–organic thin-film materials.[13,17–23] For an efficient TE device, both n- and p-type thermoelectric (semi)conductive material components are needed. The goodness of these materials is measured by the so-called figure-of-merit ($ZT = S^2 T/\rho\kappa$) which is maximized at each operation temperature (T) by increasing the magnitude of Seebeck coefficient (S) and electrical conductivity ($1/\rho$) and minimizing the thermal conductivity (κ).[24,25]

Having the eye on such wearable devices, coating of textile fibers with TE thin-film materials has been challenged in several studies.[17,26–29] Conductive polymers form the most common material family used in combination with fibers due to their ease of fabrication.[30,31] Indeed, in the simplest case the fibers may be immersed in a solution containing the polymer in dissolved form. On the contrary, the so-called PEDOT:PSS (poly(3,4-ethylenedioxythiophene):polystyrene sulfonate) coating is typically produced by methods such as vapor phase polymerization,[15] stencil printing[32] or in situ polymerization.[16] Most of the conductive polymers are p-type materials. Efforts to develop n-type conductive polymers have typically focused on combining PEDOT:PSS with different materials such as poly(3-hexylthiophene-2,5-diyl),[27] poly[Na(NiETT)],[32] and multiwalled carbon nanotubes plus poly(N-vinylpyrrolidone).[33] Moreover, carbon nanotubes have been used as both p- and n-type materials on fibers,[34] or with graphene oxide.[35] So far, though, the performance of the n-type polymers and related carbon-based materials has remained inferior in comparison with their p-type counterparts.

For the n-type TE component, inorganic compounds would possess superior TE characteristics;[36,37] they are, however, rigid and difficult to be integrated with flexible substrates. Here, one of the intriguing approaches is to fabricate inorganic–organic

hybrids such as superlattice (SL) thin films.[19,38] When considering the flexibility and complex substrate morphology, e.g., textile fibers or nanocellulose, the atomic layer deposition (ALD) thin-film technology has unique advantages.[39–41] With ALD it is possible to coat the fibers through a relatively low-temperature process in a conformal manner so that the textile substrate becomes an active part of the device. This technique is based on two reactive gaseous (evaporated) precursors that do not self-react. These precursors are sequentially pulsed into the reactor followed by an inert gas purge pulse. By controlling the individual precursor and purge pulse lengths, it is possible to find the conditions where the precursors react only on the substrate surface and the thin film grows in a highly conformal atomic layer-by-atomic layer manner and covers homogeneously the underlining substrate surface even for complex/porous substrate structures such as those of textiles and fibers. This also ensures the accurate control of the film thickness. Moreover, within the ALD scheme, it is possible to combine organic precursors with inorganic precursors to build inorganic–organic SL structures with atomic/molecular layer accuracy; the method is then called ALD/MLD (atomic/molecular layer deposition).[39,42] The unique advantages of this approach are that the organic interlayers between the TE inorganic layers provide the films for enhanced mechanical flexibility and also multiple interfaces to efficiently block the phonon-mediated thermal conduction.[20,43]

In the current work, we demonstrate the fabrication of flexible thin-film-coated textile-based thermoelectric devices; ALD-grown ZnO films and ALD/MLD-grown ZnO-hydroquinone (ZnO-HQ) SL films are used as n-type TE components and spin-coated PEDOT:PSS as the p-type component. Zinc oxide was chosen as the n-type inorganics because of its sustainable elemental composition, low cost, low toxicity, and compatibility with low-temperature ALD processing as well as its admissible thermoelectric characteristics.[44,45] Previously, ZnO has been combined with fibers in a number of works as summarized in a recent review by Verbič et al.,[46] however, only in few studies emphasizing its thermoelectric properties.[17,47]

2. Results and Discussion

### 2.1. Device Designs and Deposition Schemes

We designed two types of device configurations, in which the temperature gradient across the thermoelectric materials is either longitudinal or vertical. Also developed and tested were different approaches for the deposition of the thermoelectric coatings on the cotton textile substrates. The p-type PEDOT:PSS coatings were fabricated by either spraying or immersion as described in Section 4; it should be emphasized that efforts were made to standardize these intrinsically less reproducible procedures (compared with the ALD and MLD processes) to avoid unnecessary thickness/quality variation. For the n-type ZnO and ZnO-organic depositions, different approaches were investigated as well, as described and discussed in the following. Mechanical properties of the devices were not systematically tested in this work. However, we recently demonstrated for ALD/MLD-grown magnetic metal oxide–organic thin films that in particular such SL films with additional organic layers

within the inorganic matrix are appreciably flexible.[48] Also, we intentionally bent our TE textile devices while handling them, both before and in between the measurements, and found them durable enough. They were also found highly stable in open air, showing no changes in their TE performance even after extended storage in air.

2.1.1. Patterning with Masks

In the first deposition approach, the thermoelectric components were directly patterned on textile during the deposition utilizing masks; an example of the final (longitudinal) device is shown in **Figure 1**. The particular capability of the ALD (and MLD) technique of coating the fibers all the way through the sample thickness is beneficial for the TE performance as it increases the thickness of the active TE pads. However, this feature also creates the challenge of finding the conditions to limit the deposition to the relevant areas of the patterned pads. In other words, for these devices the lateral diffusion needs to be limited to maintain the desired pattern. We utilized the direct selective deposition approach based on masks to find the optimal pulse times and cycle numbers for the minimal lateral film growth within the textile in general. The textile material was medium-density cotton, selected based on our preliminary tests; within the low-density textile the precursor diffusion and thereby the unwanted lateral deposition were enhanced, whereas in the case of a high-density textile longer deposition times for the precursors were needed to properly diffuse around the fibers. The optimized deposition parameters are given in the Section 4.

Figure 2 shows the testing schematics we used for the longitudinal mask-based devices. We tested two different mask configurations, i.e., one with the same open mask on both sides of the textile and another one with an open mask only on top of the textile (with a closed back plate). The plates were tightly screwed together. In addition to the different mask configurations, the deposition parameters were varied. For this we developed a setup with a stop-flow valve to close the reaction chamber for 10 s after the introduction of the precursors in the chamber. This longer stay time was expected to improve the deposition on the fibers but at the same time increase the lateral diffusion of the precursors.
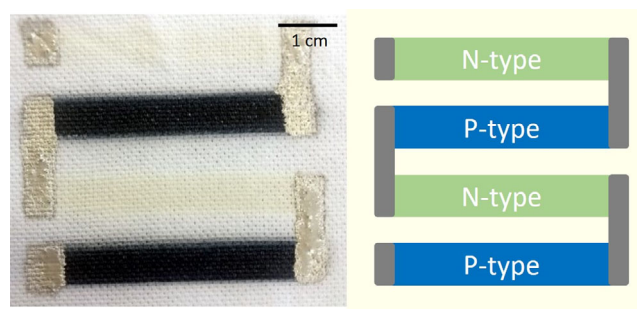
Figure 1. Longitudinal mask-patterned device design: on the left n-type (ALD ZnO, light yellow) and p-type (sprayed PEDOT:PSS, dark blue) pads and the silver paste connection; on the right, the schematics of the same design (the hot side is on the left and the cold side on the right of the sample).
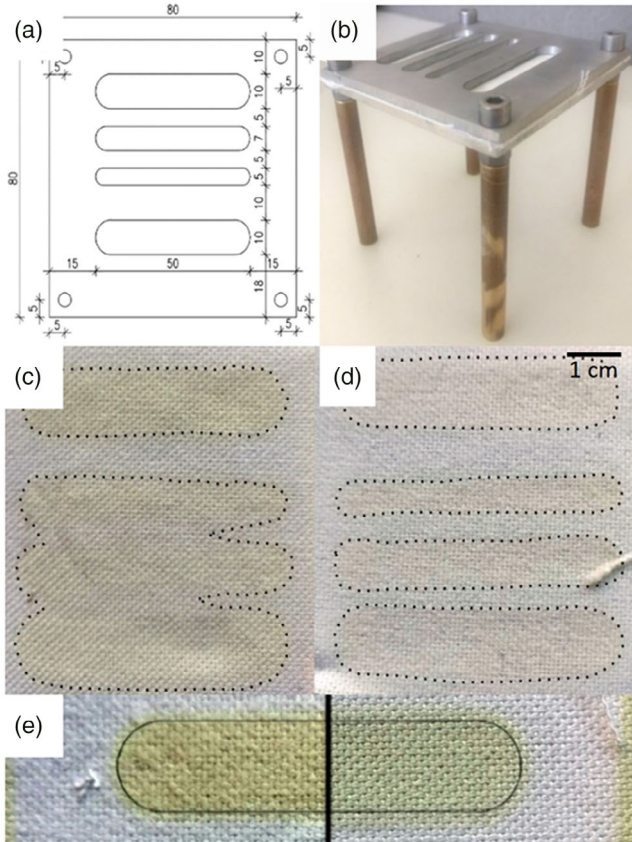
Figure 2. Selective ALD deposition testing: a) mask design with different hole dimensions and spacings; b) actual mask assembly with the textile between the plates; c) deposition result with the stop-valve pulsing (similar results observed with the open-back-plate assembly); d) deposition result with the closed-back-plate assembly; e) deposition results (closed-back-plate assembly) with 1800 (left) and 3600 (right) ALD cycles showing that the lateral diffusion is not significantly affected by the number of cycles.

It was found that the open-back-mask configuration was not effective in limiting the unwanted lateral deposition either with long or short precursor pulses (Figure 2); therefore, we selected the closed-back-mask configuration for the further experiments. With this configuration, we tested long pulses, short pulses with and without the stop-flow valve, and different number of cycles. The stop-flow valve and long pulses were again not effective at preventing the lateral deposition, so subsequent depositions were done with a closed mask and short pulses. To achieve the needed final film thickness, we tested both a long deposition from one side of the substrate and two shorter deposition of both sides of the substrate. As shown in Figure 2e, the best results were obtained with shorter depositions and the final depositions were carried out with 1800 ALD cycles on both sides of the sample.

2.1.2. Cutting of Precoated Textiles

In the second deposition approach, the p- and n-type TE materials were deposited without masking on the textile that was then cut into smaller pieces; these pieces were arranged on the textile substrate with holes in a 4×4 grid; an example of the final (vertical) device is shown in **Figure 3**. In this case there was no need to optimize the deposition, so longer pulses with the stop-flow valve were used. Samples were also deposited at both 100 and 200 °C and different thicknesses to test the difference in performances. The fabrication of the textile device was done by hand, and accordingly the reproducibility was not perfect either for the dimensions or the position of the thermoelectric pads; nevertheless, the results were satisfactory for most of the samples.

The main advantage of the precoating, cutting, and assembly design over the selective mask-based deposition is the ease of fabrication and the higher quality coating achieved on the textile. The fabrication is simple and can be scaled if needed. Electrical connection was accomplished by using conductive tape. This tape was also used to keep the TE pads attached to the substrate, and to attach thermal pads on both sides of the sample for thermal contact and added protection.
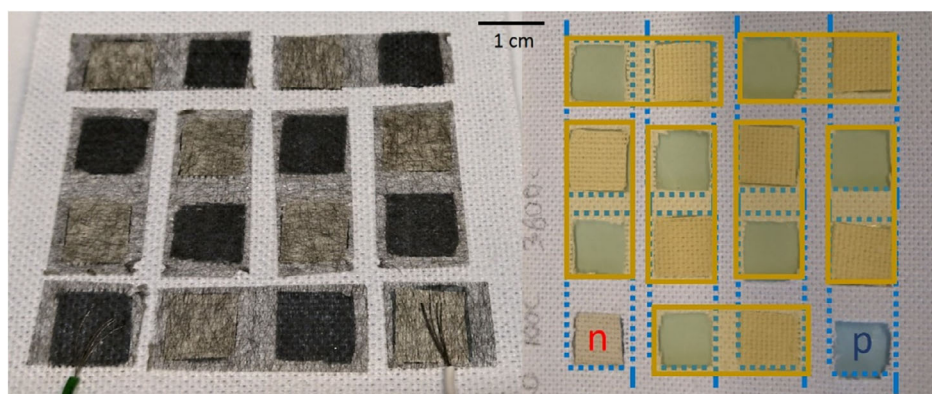
2.1.3. Device Design and Scaling-Up

In principle, the benefit of the longitudinal design is the possibility to maintain a larger temperature difference across the materials because the hot and cold sides are far apart, whereas in the vertical design the hot and cold sides are on top of each other. Here, however, the textile substrate (being the same in both designs) had a major contribution to the thermal insulation such that the two designs were not so different after all in terms of the temperature difference between the hot and cold sides. The possibility to scale up the device was tested with the vertical scheme, by increasing the number of thermoelectric couples by doubling the number of coated textile pieces (albeit half in size), i.e., by fabricating 4×8 grids of p–n couples (**Figure 4**).

2.2. Device Performance

We tested our prototype devices having the eye on their targeted use as wearable devices able to harness the heat from the human body; ultimately, we may imagine a flexible textile-based device around an arm. Here we measured voltage (V) versus temperature difference (ΔT) graphs for different device configurations to appreciate the difference of the open-circuit voltage with the temperature difference across the sample (thickness or length of the pads). The high internal resistance of the devices (measured values ranging from 12 to 110 MΩ) prevented them to drive any external load. The data collection was repeated 3 times per sample (the curves have slightly different colors in the graphs) to ensure the repeatability of the results. The heating and cooling rates were different, as the heating rate was driven by the hotplate heating up while the cooling rate was dictated only by the cooler on the cold side of the sample; in other words, the cooling was slower than the heating. In general, the heating and cooling curves were found to be consistent with occasional hysteresis, arising from variation in the cooling rate and/or the system not having good thermal equilibrium during the first run. In the following, we first present the results for the ZnO-based devices; comparison with the ZnO-HQ-based ones is then presented in the next section.

**ADVANCED
SCIENCE NEWS**

www.advancedsciencenews.com

**ADVANCED
ENGINEERING
MATERIALS**

www.aem-journal.com

Figure 3. Vertical precoated-and-cut design: on the left the final device with n- and p-type precoated pads connected by the 3M to the textile substrate tape; on the right, the assembled device and design schematics drawn on top of it; dotted blue lines and yellow lines showing where the connections will be on both sides of the textile, blue on one side and yellow on the other; hot and cold sides are on top and bottom of the sample. These are 4×4 devices with eight TE couples consisting of 16 pads of a size of $\approx 1.0\,cm^2$; active part of the device is thus $6\,cm \times 6\,cm$.
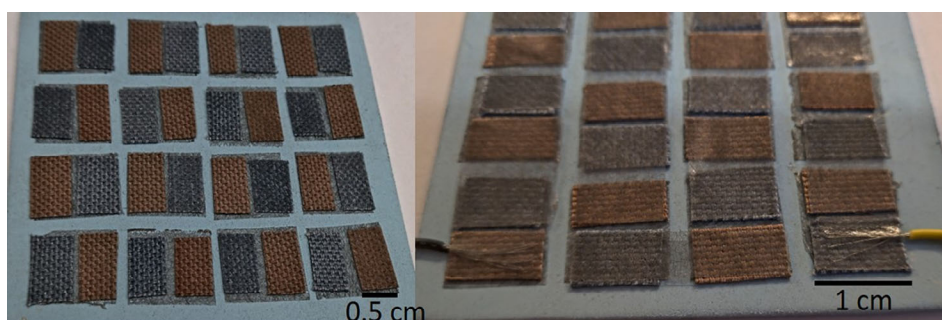
Figure 4. Devices fabricated with "smaller-in-size but larger-in-number" TE pads, i.e., 4×8 grid of n–p pairs (16 TE couples); the dark brown color of ZnO-coated textile due to the high deposition temperature (200 °C). Left: device assembled with the bottom connection that connects the n and p materials in a pair. Right: all the pairs are connected from the top side; device built directly on the thermal pad. Each pad $\approx 1\,cm \times 0.5\,cm$ in size; total active area $5\,cm \times 5\,cm$.
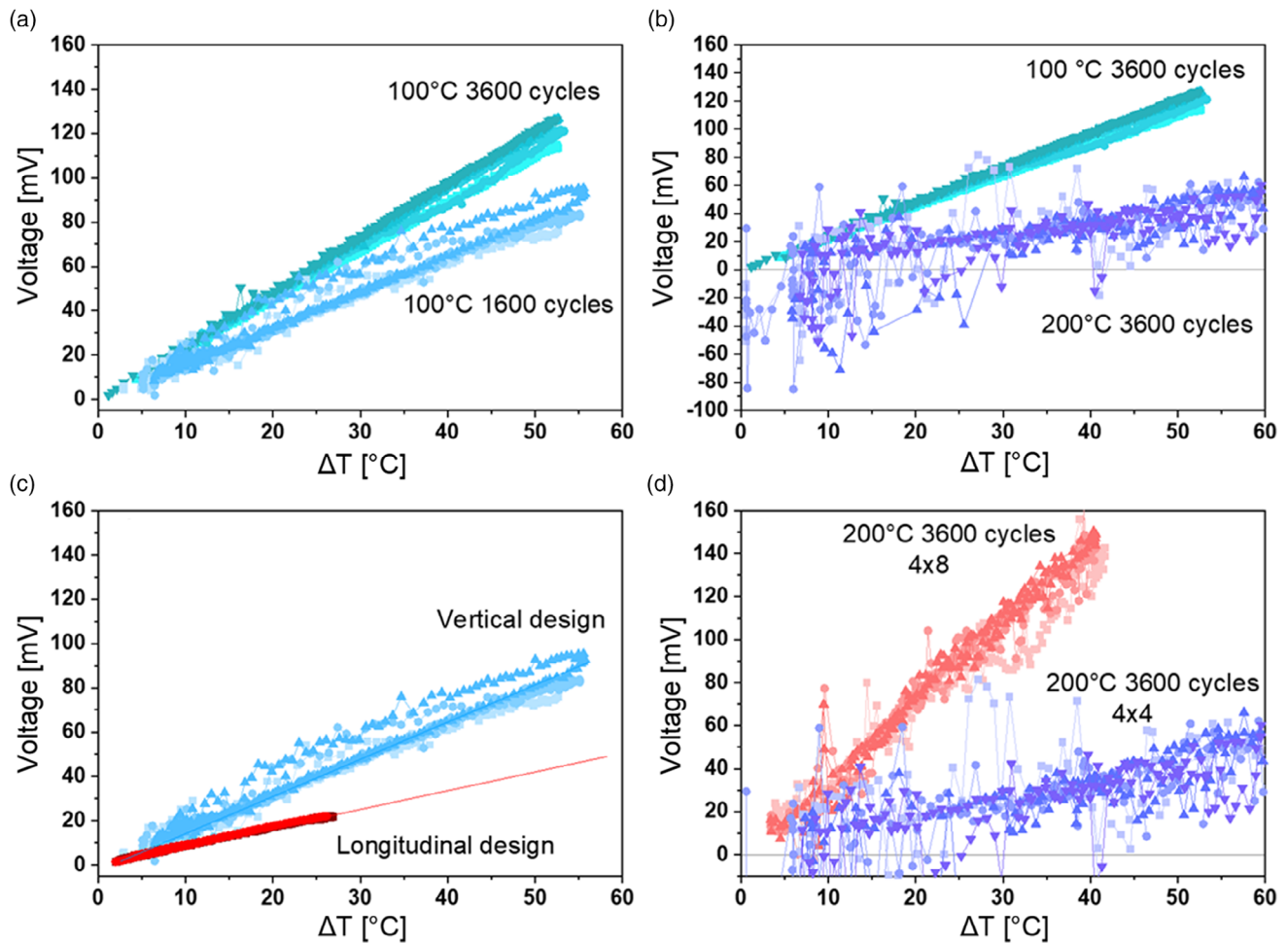
2.2.1. ZnO-Based Devices

First of all, we can see from **Figure 5**a that the voltage generated by the vertical ZnO/PEDOT:PSS device (4×4 TE pairs) depends on the ZnO film thickness, as expected. In this figure, devices based on ZnO films grown at the same temperature (100 °C) with 1600 and 3600 ALD cycles (expected thicknesses around 270 and 600 nm) are compared, and the conclusion is that the former device produces—at the same ΔT—a voltage 60% higher than the latter one. However, it tentatively looks that the increase in the performance is not linear; this is understandable because the film grows also within the fibers of the textile substrate.

In Figure 5b, the V–ΔT curves for devices based on the ZnO films deposited at different temperatures (100 and 200 °C) are shown. From this comparison, it seems that the lower deposition temperature leads to the better thermoelectrical characteristics of the material, as not only the produced voltage is higher but also less oscillation of the data points is seen. The reason for this is not fully understood. From previous studies it is known that the preferred orientation of polycrystalline ZnO films grown by ALD on, e.g., silicon substrate depends on the deposition temperature.[44] However, the film orientation should not be so critical when growing on textile because the film is growing

all around the fibers and within the whole substrate thickness. It is also possible that the higher deposition temperature (200 °C) has somehow already affected the textile substrate.

The performance difference between the longitudinal and vertical designs can be seen from Figure 5c; clearly, the vertical design produces—by a factor of two—higher voltages. The vertical design is composed of two TE couples, each n- and p-type leg being $\approx 1\,cm^2$ in area, and the textile thickness being 2 mm. In the longitudinal design ($1 \times 6\,cm$), there are less TE couples in the same device area (two instead of eight couples; one longitudinal leg needs a similar area as four vertical legs) which most probably is the reason for the lower voltage generation. Apparently, owing to its larger area one longitudinal TE couple produces higher voltage than a vertical TE couple, but then in the entire device, the vertical design can accommodate more TE couples per area and yield higher voltage. As the vertical design yielded better results, it was then used in all the devices discussed unless otherwise specified.

The initial motivation to challenge the longitudinal design was to be able to maintain a larger ΔT more easily between the hot and the cold ends, but apparently this did not translate into the better performance in practice. The vertical design can maintain a similar ΔT, but it needs a high and constant heating

**ADVANCED
SCIENCE NEWS**

www.advancedsciencenews.com

**ADVANCED
ENGINEERING
MATERIALS**

www.aem-journal.com

Figure 5. Samples (2 mm-thick cotton substrate) with ZnO films using vertical design in all but graph c. a) Comparison of the effect of thickness with ZnO deposited at 100 °C; b) effect of deposition temperature of samples with the same amount of ALD cycles; c) comparison between the different device design with ZnO deposited at the same temperature and similar cycles; d) comparison between the 4 × 4 thermoelectric legs device and the 4 × 8 device with similar temperature and deposition cycles.

temperature to achieve the best performance. This is due to the short distance between the hot and cold sides that causes faster heat transfer in the whole device area. The longer distance between the hot and cold sides in the longitudinal design, in the order of centimeters, is better suited to maintain the temperature difference for longer, such that the constant heating is not necessarily required. The main shortcoming of the longitudinal device is the large area required for each TE couple; therefore, when the device area is kept constant, the vertical design will produce higher voltage due to the larger number of TE couples. More tests are, however, needed to thoroughly understand the behaviors of the two designs in different heating conditions.

To further enhance the performance of our devices by increasing the TE couple density, smaller pads were cut to double the number of pairs in a given device area. In Figure 5d, the graphs are showing the difference between a 4 × 4 grid and a 4 × 8 grid of ZnO pads. The higher voltage produced by the 4 × 8 device arises from the higher number of TE couples. Most importantly, the voltage of the 4 × 8 device is higher for the whole ΔT range with the slope of the linear fit being 3 times higher than in the

case of the 4 × 4 device. Finally, it should be noted that in both cases the ZnO pads were deposited at 200 °C, which could lower the overall performance of the devices, but presumably in parallel fashion; this also underlines one of the ways to easily improve our demonstration devices further.

To get an idea of the power generated by the devices, we calculated the maximum power (P_{max}) as

$$P_{max} = \frac{V_0^2}{4R_i} \tag{1}$$

from the open-circuit voltage (V_0) at a certain ΔT (40 °C) and the internal resistance (R_i) of the device. For the ZnO-based devices P_{max} was found to be 3 and 70 pW for the following devices: (200 °C; 3600 cycles; 4 × 4) and (200 °C; 3600 cycles; 4 × 8), respectively. In the latter case, the power per area was 5.8 pW cm^{-2}.

2.2.2. Devices Based on ZnO-HQ SLs

In **Figure 6**, we show the performances of different devices fabricated using the ZnO-HQ SL thin films grown by ALD/MLD.
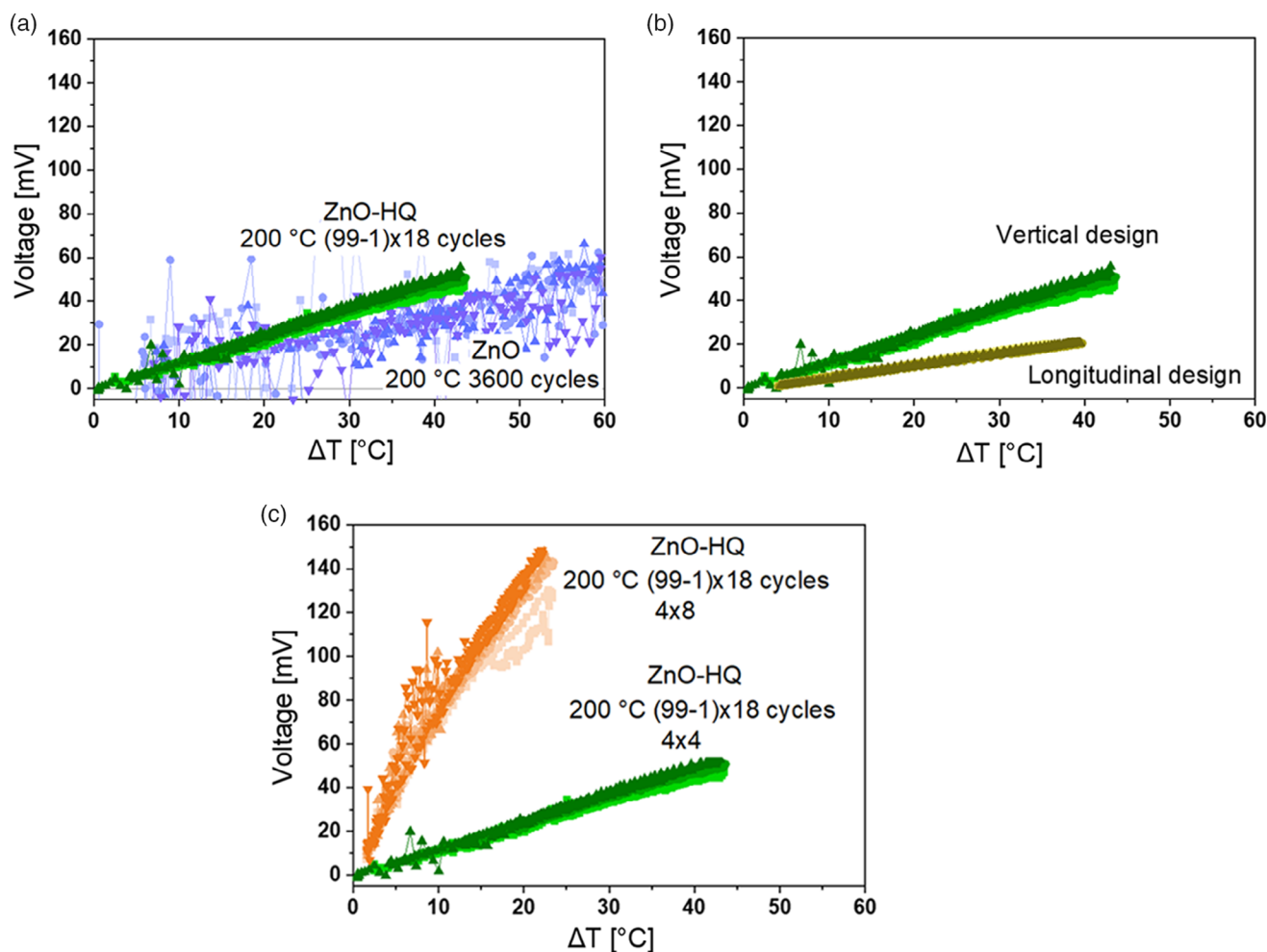
Figure 6. Samples with ZnO-HQ SLs using vertical design in both graphs a and c. a) Comparison between the SL (1800 cycles) in green and the ZnO (3600 cycles) in purple, both deposited at 200 °C, the ZnO (1600 cycles) deposited at 100 °C for complete comparison; b) vertical and longitudinal designs utilizing similar SL films; c) comparison between the ZnO-HQ 4 × 4 and 4 × 8 devices deposited at the same temperature and with the same cycles.

First, in Figure 6a we compare our ZnO-HQ-based device where the ZnO-HQ pads were grown with 1800 ALD/MLD cycles with a ZnO device with similar configuration but with thicker n-type TE pads (grown with 3600 ALD cycles); in both cases the deposition temperature was 200 °C. It can be seen that the ZnO-HQ device performs essentially better than the ZnO device, even though the coating thickness is half in the former case. From our previous works,[20,43,49] ZnO-HQ SLs showed significantly lower thermal conductivity values and higher Seeback coefficients with only slightly higher resistivity compared with the parent ZnO thin films. Indeed, the present results showing the higher output voltage for the ZnO-HQ SL devices verify that the superior TE characteristics of the SL films apply also in the device scale and in the case of textile substrates. Furthermore, it is seen that the voltage produced by the ZnO-HQ SL device remains stable with minimum oscillations confirming the successful fabrication.

From Figure 6b, similarly as in the case of the ZnO-based devices, the vertical design is preferable over the longitudinal

design also with the ZnO-HQ SL case. Finally, from Figure 6c we can see that doubling the number of TE legs yields higher voltages also for the ZnO-HQ devices. Most impressively, the voltage produced by the ZnO-HQ 4 × 8 device is ≈150 mV compared with ≈90 mV of the ZnO 4 × 8 device at the same ΔT with a slope of the linear fit being almost 5 times higher. Again, this is demonstrating the superior performances of the ZnO-HQ SLs even when the thickness of the ZnO-HQ coating is almost half of the thickness of the ZnO coating. It should also be emphasized that the maximum voltage of 150 mV generated here is substantially higher compared with the output (in μV level) achieved in our previous work for devices grown on nonporous flexible plastic and glass substrates.[26]

Similarly as before, the power generated by the device utilizing the Zn-HQ SLs was measured at $\Delta T = 20$ °C for both the 4 × 4 (13 pW) and 4 × 8 (38 pW) devices. The 4 × 4 device generated 33 pW at $\Delta T = 40$ °C. The highest power per area was 3.2 pW cm^{-2} for the 4 × 8 device at $\Delta T = 20$ °C.

**ADVANCED
SCIENCE NEWS**

www.advancedsciencenews.com

**ADVANCED
ENGINEERING
MATERIALS**

www.aem-journal.com

2.2.3. Considerations for Further Improvements

In the literature, few reports of textile-based thermoelectric devices are found. For example, the wearable device reported by Allison et al. based on PEDOT-coated fibers produced a voltage of 20 mV when worn on the hand, i.e., with a relatively small ΔT.[11] On the other hand, the device fabricated by Lee et al. based on Bi_2Te_3- and Sb_2Te_3-coated fibers produced powers up to $8.6\,W\,m^{-2}$ when the ΔT was $200\,°C$.[50] Devices on textile utilizing organic coatings are generally found to produce power outputs in the nW range.[27,30,51] Compared with these literature examples, our devices produced a lower power, in the order of pW, but with a high open-circuit voltage of $\approx100\,mV$ and with a ΔT of only $60\,°C$. The combination of oxide n-type and organic p-type does not perform at the same level of the traditional ceramic TE materials, but offers higher flexibility and ease of fabrication. With lower electrical resistance in the materials, the generated voltage would rise, and the devices could drive an external load as well as produce powers in the nW range, similar to the textile devices found in the literature.

From the experiments with the ZnO-based devices we noted that the voltage produced by the ZnO films deposited at $100\,°C$ was superior to those deposited at $200\,°C$. The higher deposition temperature used in ALD might negatively influence the cotton textile substrate and thereby the overall thermoelectric performance because the textile is part of the active device. Indeed, a color change was seen for the textile when the high deposition temperature was used. It should be noted that the TE ALD-ZnO coating thickness is in the $300–500\,nm$ range, whereas coating textile fibers with diameters are in the $100\,\mu m$ range so the thermal conductivity is dominated by the textile material. Unfortunately, in the case of the ALD/MLD process for ZnO-HQ the high sublimation temperature of the HQ precursor limits the deposition temperature to $150\,°C$ at the lowest,[17–19] but the higher $180\,°C$ is used for optimal results in the reactor. In future, it will be interesting to challenge other organic precursors with lower sublimation temperatures for the preparation of the ZnO-organic SL coatings to reach the optimized performance of our test devices.

Another variable that will require more study is the PEDOT: PSS as the p-type material. In most of the devices investigated, the PEDOT:PSS was sprayed on the textile and the thickness of the layer could not be accurately controlled. Similarly, the immersion coating method also tested for PEDOT:PSS, which was not able to provide us with more accurate thickness control. Moreover, the PEDOT:PSS films were thicker than the ALD and ALD/MLD films. Fortunately, in this work this seemed not to affect over the conclusions made for the optimization of the n-type ALD and ALD/MLD components because the thickness of the p-type PEDOT:PSS films, although not known, was consistent in all the samples.

An optimization of the ALD/MLD deposition on the textiles, different textiles that might resist better to high deposition temperature and improved connections between the TE pads, could contribute to the reduction of the internal resistance of the devices.

3. Conclusions

In this work we have demonstrated the feasibility of thermoelectric textile devices fabricated using the state-of-the-art ALD technology for high-quality inorganic thin films and coatings, and its strongly emerging variant ALD/MLD for unique inorganic–organic hybrid materials. One of the attractive features of both the ALD and the combined ALD/MLD techniques is their capacity to coat the fibers in a conformal manner so that the textile substrate becomes an active part of the device.

Two device designs, longitudinal and vertical, were tested in this work, with the latter showing better performances and thus being chosen for the majority of the experiments. The final devices could maintain a ΔT up to $50\,°C$ between the hot side on a hotplate and the cold side in contact with the cooler. This was more than enough to test the potential of these flexible/wearable devices to be powered by body heat, as imagined to be the case in their future usage scenario.

In our device tests we demonstrated how both the film thickness and deposition temperature affect the TE performances with the thicker coatings performing better than the thinner ones as expected. The lower deposition temperature ($100\,°C$) turned out to be more favorable than the higher ($200\,°C$) for ZnO. We also demonstrated that the devices behaved as expected when the number of TE pairs was doubled; quite promisingly, the voltage produced was enhanced by up to 5 times. The maximum power generated by the devices was in the order of tens of pico-Watts, a low value that is nevertheless demonstrating the functionality of TE thin films on textile. A reduction of the internal resistance could increase the generated power by an order of magnitude.

Finally, we revealed enhanced performances for the devices where ZnO-HQ SL coatings were used as the n-type component instead of the ZnO films. These devices reached a maximum of 150 mV generated with a ΔT of $25\,°C$. This is remarkable, as these hybrid inorganic–organic materials are also mechanically more flexible, and thus better suited to the flexible/wearable energy harvesting applications in combination with textiles.

4. Experimental Section

All the precursors were commercial chemicals; diethyl zinc (DEZ; $\geq52\,wt\%$ Zn basis, $\geq99\%$, Aldrich), trimethyl aluminum (TMA; 97%, $\geq99\%$, Aldrich), and DI water were used for the ALD depositions of ZnO and Al_2O_3 films, hydroquinone (HQ; $\geq99\%$, Aldrich) as the organic component in the hybrid ALD/MLD cycles of the ZnO-HQ films, and PEDOT:PSS (1% in water, Heraeus) for the p-type coating on the fibers. All the precursors were stored and used at room temperature except for hydroquinone that was heated to $180\,°C$ during deposition to reach the sublimation temperature. The textile material used as the substrate was of 100% cotton (prewashed furniture fabric Matias from Eurokangas; $250\,g\,m^{-2}$). The ALD and MLD depositions were performed in a Picosun R-100 top flow reactor with Nitrogen carrier gas (produced with a Parker HP 5000 N2 generator, oxygen content less than 10 ppm).

ALD and MLD Experiments: The ALD and MLD films were grown at either 100 or $200\,°C$ with different recipes depending on the fabrication route, vertical or longitudinal designs. In all depositions, a thin (100 cycles) layer of Al_2O_3 was first deposited prior to the TE film (ZnO or ZnO-HQ) deposition to improve the growth on the fibers; note that Al_2O_3 grows easier on cotton fibers compared with ZnO, and the initial Al_2O_3 layer is beneficial to the ZnO growth.[17,52] The layer of Al_2O_3 was deposited

**ADVANCED
SCIENCE NEWS**

www.advancedsciencenews.com

**ADVANCED
ENGINEERING
MATERIALS**

www.aem-journal.com

on all the samples with the same growth parameters: 0.2 s for TMA and 0.5 s for water. The SL was deposited at 200 °C because of the required 180 °C sublimation temperature of the hydroquinone precursor in addition to the higher temperature needed for the organic layer growth. The optimized precursor pulse lengths used (unless otherwise stated) were the same for all the samples, 0.2 s for DEZ and 0.3 s for water with a 20 s purge in both cases. The pulses for the hydroquinone precursors were 10 s with 20 s purge. Some depositions were tested with longer 1 s pulse for both DEZ and water and 15 s purges.

Assembly of the device from predeposited p and n textiles changed the preparation pipeline. There was no need for masking certain areas of the substrate, so the pulse times could be lengthened by adding the staying time of the precursors inside the chamber. This used the stop-flow valve giving the precursor the needed time to diffuse inside the whole thickness of the substrate and conformally coats all the fibers' surface area. Pulse times for DEZ/water were 0.2/0.5 s with a hold time of 10 s and a purge of 20 s.

The SL samples were prepared following the structure of 99 cycles of DEZ/water and 1 of hydroquinone/DEZ. This sequence is repeated 16 times to obtain the final structure. In the vertical design, 18 repetitions of the SLs were used.

PEDOT:PSS Depositions: The PEDOT:PSS coatings were fabricated by either spraying or immersion depending on the device fabrication method. Spraying was used when the pattern was made directly on the device after ALD deposition utilizing a similar mask. The spray was tested before the fabrications of the samples and the final spray was done with five layers (next layer sprayed after the previous one was dry) on each side of the textile. When spraying on the same side, more than eight layers were not improving the consecutive characteristics of the PEDOT film while not reaching fully the other side. The immersion method was utilized to coat a larger area of textile that was then cut into the smaller pieces for assembly in the final device in combination with the ALD-coated textile pieces. The immersion time of the textile substrate in the PEDOT–water solution was kept constant (1 min total immersion time, turning the sample around after 30 s) in all experiments to achieve constant coating thickness/quality.

Device Fabrication: For the devices fabricated directly on the substrate with the selective area deposition, the n-type areas were patterned during the ALD film growth with a mask that was open on one side of the substrate and closed on the other side. The two sides of the masks were tightened to each other on the corners. To complete the device, the p-type PEDOT:PSS pads were sprayed on the needed areas through another mask.

In the other device fabrication scheme based on an assembly of precoated textile parts into a precut textile, both the n-type (ALD ZnO or ALD/MLD ZnO-HQ) and the p-type (PEDOT:PSS) textiles were cut into

size and kept in place by the electrically conductive double-sided 3M 9719 tape. The tape is conductive along both the *xy*-axis and *z*-axis directions to provide the necessary connections between the pads on both sides of the device completing the circuit. At the same time, the tape allows us to keep the different parts of the device together and attach the thermal pads on both sides of the device.

Device Testing: The devices were tested on a hotplate as the hot side (with a temperature range of 30–170 °C), whereas the temperature of the cold side was maintained by a CPU cooler on top of the device (**Figure 7**). The temperature difference was measured with two resistive thermometers attached to the hot and cold side of the device. Thermal pads were placed in between to prevent electrical contact and ensuring the best thermal contact. The voltage produced by the device was collected by another multimeter to be plotted in the V–ΔT graphs.

Conflict of Interest

The authors declare no conflict of interest.

Keywords

atomic layer deposition, devices, textiles, thermoelectric, thin films

[1] C. Sa, X. Xu, X. Wu, J. Chen, C. Zuo, X. Fang, *J. Mater. Chem. C* **2019**, *7*, 13097.

[2] S. Cai, X. Xu, W. Yang, J. Chen, X. Fang, *Adv. Mater.* **2019**, *31*, 1808138.

[3] X. Xu, J. Chen, S. Cai, Z. Long, Y. Zhang, L. Su, S. He, C. Tang, P. Liu, H. Peng, X. Fang, *Adv. Mater.* **2018**, *30*, 1803165.

[4] B. Zhao, F. Wang, H. Chen, L. Zheng, L. Su, D. Zhao, X. Fang, *Adv. Funct. Mater.* **2017**, *27*, 1700264.

[5] S. Bodkhe, C. Noonan, F. P. Gosselin, D. Therriault, *Adv. Eng. Mater.* **2018**, *20*, 1800206.

[6] H. C. Koydemir, A. Ozcan, *Annu. Rev. Anal. Chem.* **2018**, *11*, 127.

[7] R. Paradiso, G. Loriga, N. Taccini, *IEEE Trans. Inf. Technol. Biomed.* **2005**, *9*, 337.

[8] M. Yoshimoto, S. Izumi, *IEICE Trans. Electron.* **2019**, *E102.C*, 245.

[9] I. Awolusi, E. Marks, M. Hallowell, *Autom. Constr.* **2018**, *85*, 96.

[10] H. Wu, Y. Huang, F. Xu, Y. Duan, Z. Yin, *Adv. Mater.* **2016**, *28*, 9881.

[11] L. K. Allison, T. L. Andrew, *Adv. Mater. Technol.* **2019**, *4*, 1800615.

[12] A. Nozariasbmarz, H. Collins, K. Dsouza, M. H. Polash, M. Hosseini, M. Hyland, J. Liu, A. Malhotra, F. M. Ortiz, F. Mohaddes, V. P. Ramesh, Y. Sargolzaeiaval, N. Snouwaert, M. C. Öztürk, D. Vashaee, *Appl. Energy* **2020**, *258*, 114069.

[13] R. Tian, C. Wan, N. Hayashi, T. Aoai, K. Koumoto, *MRS Bull.* **2018**, *43*, 193.

[14] M. Magno, D. Boyle, in *Int. Conf. on Design & Technology of Integrated Systems In Nanoscale Era*, **2017**, pp. 1–6.

Figure 7. Measurement setup with the sample between the hotplate and the cooler and the resistors measuring the temperatures at the hot and cold sides. The device is connected to another multimeter that measures the voltage output.

[15] Y. Jia, L. Shen, J. Liu, W. Zhou, Y. Du, J. Xu, C. Liu, G. Zhang, Z. Zhang, F. Jiang, *J. Mater. Chem. C* **2019**, *7*, 3496.

[16] N. A. Khoso, A. Ahmed, H. Deb, S. Tian, X. Jiao, X. Y. Gong, J. Wang, *Org. Electron.* **2019**, *75*, 105368.

[17] A. J. Karttunen, L. Sarnes, R. Townsend, J. Mikkonen, M. Karppinen, *Adv. Electron. Mater.* **2017**, *3*, 1600459.

[18] T. Tynell, M. Karppinen, *Thin Solid Films* **2014**, *551*, 23.

[19] T. Tynell, I. Terasaki, H. Yamauchi, M. Karppinen, *J. Mater. Chem. A* **2013**, *1*, 13619.

[20] F. Krahl, A. Giri, J. A. Tomko, T. Tynell, P. E. Hopkins, M. Karppinen, *Adv. Mater. Interfaces* **2018**, *5*, 1701692.

[21] C. Wan, R. Tian, M. Kondou, R. Yang, P. Zong, K. Koumoto, *Nat. Commun.* **2017**, *8*, 1.

[22] R. Tian, C. Wan, Y. Wang, Q. Wei, T. Ishida, A. Yamamoto, A. Tsuruta, W. Shin, S. Li, K. Koumoto, *J. Mater. Chem. A* **2017**, *5*, 564.

[23] H. Jin, G. Marin, A. Giri, T. Tynell, M. Gestranius, B. P. Wilson, E. Kontturi, T. Tammelin, P. E. Hopkins, M. Karppinen, *J. Mater. Sci.* **2017**, *52*, 6093.

[24] H. J. Goldsmid, *Introduction to Thermoelectricity* (Ed: H. J. Goldsmid), Springer, Berlin, Heidelberg, **2016**, pp. 9–84.

[25] G. J. Snyder, in *Frontiers in Electronic Materials*, John Wiley & Sons, Ltd, **2013**, p. 44.

[26] G. Marin, T. Tynell, M. Karppinen, *J. Vac. Sci. Technol. A* **2019**, *37*, 020906.

[27] J. Pope, C. Lekakou, *Smart Mater. Struct.* **2019**, *28*, 095006.

[28] J. S. Jur, W. J. Sweet, C. J. Oldham, G. N. Parsons, *Adv. Funct. Mater.* **2011**, *21*, 1993.

[29] C. Müller, L. Ouyang, A. Lund, K. Moth-Poulsen, M. M. Hamedi, *Adv. Mater.* **2019**, *31*, 1807286.

[30] A. Lund, N. M. van der Velden, N.-K. Persson, M. M. Hamedi, C. Müller, *Mater. Sci. Eng. R Rep.* **2018**, *126*, 1.

[31] J. D. Ryan, D. A. Mengistie, R. Gabrielsson, A. Lund, C. Müller, *ACS Appl. Mater. Interfaces* **2017**, *9*, 9045.

[32] H. M. Elmoughni, A. K. Menon, R. M. W. Wolfe, S. K. Yee, *Adv. Mater. Technol.* **2019**, *4*, 1800708.

[33] J. D. Ryan, A. Lund, A. I. Hofmann, R. Kroon, R. Sarabia-Riquelme, M. C. Weisenberger, C. Müller, *ACS Appl. Energy Mater.* **2018**, *1*, 2934.

[34] F. Islam, A. Zubair, N. Fairuz, in *IEEE Student Conf. Research and Development SCOReD*, IEEE, Bandar Seri Iskandar **2019**, pp. 253–258.

[35] C. Cho, N. Bittner, W. Choi, J.-H. Hsu, C. Yu, J. C. Grunlan, *Adv. Electron. Mater.* **2019**, *5*, 1800465.

[36] R. Funahashi, T. Mikami, T. Mihara, S. Urata, N. Ando, *J. Appl. Phys.* **2006**, *99*, 066117.

[37] A. Inagoya, D. Sawaki, Y. Horiuchi, S. Urata, R. Funahashi, I. Terasaki, *J. Appl. Phys.* **2011**, *110*, 123712.

[38] J.-P. Niemelä, A. J. Karttunen, M. Karppinen, *J. Mater. Chem. C* **2015**, *3*, 10349.

[39] S. M. George, *Chem. Rev.* **2010**, *110*, 111.

[40] M. Leskelä, M. Ritala, *Thin Solid Films* **2002**, *409*, 138.

[41] G. N. Parsons, S. M. George, M. Knez, *MRS Bull.* **2011**, *36*, 865.

[42] P. Sundberg, M. Karppinen, *Beilstein J. Nanotechnol.* **2014**, *5*, 1104.

[43] T. Tynell, A. Giri, J. Gaskins, P. E. Hopkins, P. Mele, K. Miyazaki, M. Karppinen, *J. Mater. Chem. A* **2014**, *2*, 12150.

[44] J. Malm, E. Sahramo, J. Perälä, T. Sajavaara, M. Karppinen, *Thin Solid Films* **2011**, *519*, 5319.

[45] T. Tynell, M. Karppinen, *Semicond. Sci. Technol.* **2014**, *29*, 43001.

[46] A. Verbič, M. Gorjanc, B. Simončič, *Coatings* **2019**, *9*, 550.

[47] P. Veluswamy, S. Sathiyamoorthy, P. T. Gomathi, K. Jayabal, R. Kumar, D. Kuznetsov, H. Ikeda, *Appl. Surf. Sci.* **2019**, *496*, 143658.

[48] A. Philip, J.-P. Niemelä, G. C. Tewari, B. Putz, T. E. J. Edwards, M. Itoh, I. Utke, M. Karppinen, *ACS Appl. Mater. Interfaces* **2020**, *12*, 21912.

[49] A. Giri, J.-P. Niemelä, C. J. Szwejkowski, M. Karppinen, P. E. Hopkins, *Phys. Rev. B* **2016**, *93*, 024201.

[50] J. A. Lee, A. E. Aliev, J. S. Bykova, M. J. de Andrade, D. Kim, H. J. Sim, X. Lepró, A. A. Zakhidov, J.-B. Lee, G. M. Spinks, S. Roth, S. J. Kim, R. H. Baughman, *Adv. Mater.* **2016**, *28*, 5038.

[51] Y.-S. Chen, B.-J. Lwo, *Coatings* **2019**, *9*, 831.

[52] J. Malm, E. Sahramo, M. Karppinen, R. H. A. Ras, *Chem. Mater.* **2010**, *22*, 3349.